Soft Matter

Cite this: *Soft Matter*, 2012, **8**, 7292

www.rsc.org/softmatter

REVIEW

Stimuli-responsive polymers grafted to nanopores and other nano-curved surfaces: structure, chemical equilibrium and transport

Mario Tagliazucchi and Igal Szleifer*

Received 2nd April 2012, Accepted 30th April 2012
DOI: 10.1039/c2sm25777g

This review discusses the properties of macromolecular layers on nano-curved surfaces, with special emphasis on the fast-growing field of polymer- and polyelectrolyte-modified nanopores and nanochannels. Organization in soft materials emerges from the competition between physical and chemical interactions acting on different length scales; the geometry of the system modulates this competition and, hence, dictates its structure and function. Theoretical studies of molecular organization in planar and curved geometries require the treatment of the coupling between interactions, chemical equilibrium and geometrical constraints. We analyse here how curvature affects the morphology of polymers on nano-curved surfaces and determines the apparent equilibrium constants of surface-confined chemical reactions, such as acid–base chemistry. We also review the practical implications of introducing soft materials into nanofluidic devices. In particular, we present and discuss recent theoretical studies and simulations of the transport of ions, solvent and large cargoes through polyelectrolyte-brush-modified pores. We believe that this basic understanding will guide experimental efforts towards the design of stimuli-responsive nanopore gates.

1. Introduction

Nanometre-curved surfaces are ubiquitous in biological systems and nanotechnology: nanoparticles and nanotubes, nanochannels and meso/nanoporous materials exhibit surfaces with radii of curvature in the nanometre to hundreds-of-nanometres range. Soft materials are typically introduced to these surfaces in

Department of Chemistry, Department of Biomedical Engineering and Chemistry of Life Process Institute, Northwestern University, 2145 Sheridan Road, Evanston, Illinois, 60208-3100, USA. E-mail: igalsz@northwestern.edu

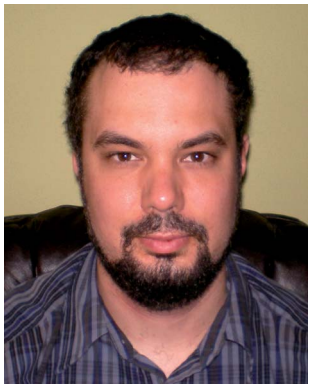

Mario Tagliazucchi

Mario Tagliazucchi was born in Buenos Aires, Argentina, in 1979. He received his degree in Chemistry from the University of Buenos Aires (UBA) in 2004 and obtained his PhD in Chemistry from the same University in 2009 under the supervision of Prof. Ernesto J. Calvo. He is currently a postdoctoral researcher at the Non-equilibrium Research Center at Northwestern University working with Professors Igal Szleifer and Emily Weiss. He has been awarded with CONICET-FUDETEC and Fulbright fellowships. His research is focused in theoretical and experimental studies in soft and hybrid materials.

Igal Szleifer

Igal Szleifer is the Christina Enroth-Cugell Professor of Biomedical Engineering and he is a Professor of Chemistry, Chemical and Biological Engineering and Medicine. His work concentrates on the development of theoretical approaches to understand the coupling that exists between molecular organization and function. His studies on molecular modeling of complex multi-component systems have applications in a range of systems ranging from responsive materials to biophysics. The understanding of the complexity of chemical reactions, physical interactions and their role in biological and biomimetic environments is at the center of his research interests.

order to confer functionality. In particular, nanopores and nanochannels coated by stimuli-responsive supramolecular species, like polymers, polyelectrolytes or surfactant layers, have recently emerged as outstanding candidates for the fabrication of molecular gates. In these systems, the curvature of the surface is commensurable with the size of the grafted macromolecules and the length scales of the intermolecular interactions. Therefore, curvature critically impacts on the properties of the system and controls its structure and function.

This review discusses the coupling between the properties of soft materials and the curvature of the immobilizing surface. Our goal is the fundamental understanding of these systems. In particular, we focus here on recent theoretical work on nanochannels and nanopores, but also address other nano-curved surfaces (such as nanoparticles and nanotubes) in order to provide a more complete and consistent description of curvature effects. We mainly describe short polymers ($n \approx 10$ to 100) and long alkyl-chain molecules, because (as we discuss below) the modification of the inner surfaces of pores and channels with long polymers is a very challenging task due to nanoconfinement effects. We refer the reader to recent review articles devoted to specific systems: stimuli-responsive polymer materials,[1] ligand-coated nanoparticles,[2–4] polymer-stabilized carbon nanotubes,[5] polyelectrolyte modified nanopores,[6] spherical polyelectrolyte brushes,[7] hairy nanoparticles,[8] macromolecule-modified nano/mesopores,[9] solid-state nanopores[10–12] and the nuclear pore complex.[13]

The difference between planar and curved surfaces is that for planar surfaces the available volume remains constant as the distance from the surface increases. On the other hand, for curved convex (concave) objects the available volume increases (decreases) as the distance to the surface increases. More specifically, the volume element at a distance r from the surface scales as $(r/R)^2$ for spheres and spherical holes, as (r/R) for cylinders, pores and channels and it is constant for planar surfaces (here R is the radius of curvature of the surface). The simplicity of this argument is, however, deceiving: the molecular organization in soft materials depends on the competition among multiple physical and chemical interactions acting on different length scales (such as van der Waals and electrostatic forces and acid–base equilibrium, to name just a few). Curvature effects modulate this competition and, thus, the optimal organization of the system will non-trivially depend on its geometry. This concept is discussed in the first two sections where we review the effect of highly curved surfaces on the morphology of end-grafted polymer layers and surface-confined reaction equilibria, respectively. In the last section, we focus on the coupling between curvature and functional properties by analysing molecular transport through polymer- and polyelectrolyte-modified nanopores and nanochannels. An important part of the theoretical insights we describe in this and following sections were gained from a molecular theory developed in our group in order to study the molecular organization and thermodynamic properties of confined polymers in general[14] and, more relevant to this review, neutral polymers and weak polyelectrolytes grafted to surfaces of different curvature.[14,15] The molecular theory methodology explicitly considers the geometry of the system, the shape, charge, charge distribution, conformations and molecular volume of all molecular species, the electrostatic and non-electrostatic interactions among them and the presence of coupled chemical equilibrium.

2. The structure of end-grafted polymers and polyelectrolytes on curved surfaces

2.1 Structure in the good solvent regime

The most studied problem comprising polymers on curved surfaces is probably that of colloidal stabilization. The modification of nanoparticles and nanotubes (convex surfaces) with polymer layers in good solvent permits the stabilization of these nano-objects in solution.[5,16,17] Steric stabilization by polymers arises from the entropy loss that occurs when two polymer-modified surfaces approach. This decrease in entropy has two contributions: (i) the conformational entropy of the polymer (as the surfaces approach, there is a decrease in the number of allowed chain conformations) and (ii) the solvent translational entropy, *i.e.* the osmotic pressure contribution (when the polymer layers are compressed, solvent is expelled from the layers).[5] For example, the van der Waals interactions between two micron-long carbon nanotubes (CNT) can be thousands of times the thermal energy[5] and therefore bare CNT are insoluble in any solvent. However, adsorption of polymers on CNT creates an entropic barrier between their surfaces that makes CNT solutions stable.[5,18] Another example of stabilization by chain-like molecules is that of spherical nanoparticles coated by a dense layer of ligands.[2,3] These ligands form compact monolayers on planar surfaces, but on highly curved surfaces their packing is disrupted due to the increase in the available volume with increasing distance to the surface.[19–23] In a good solvent, ligand chains explore the additional space provided by the convex geometry, and therefore increase their conformational entropy by adopting non-all-*trans* conformations that are rich in gauche defects (Fig. 1). The problem of colloidal stabilization, as well as structure of polymer layers in good solvent on convex surfaces,[8,24–26] is rather well understood. On the other hand, recent theoretical work has been focused on the properties of polymers on concave surfaces, more specifically, polymer-modified nanochannels[27–30]

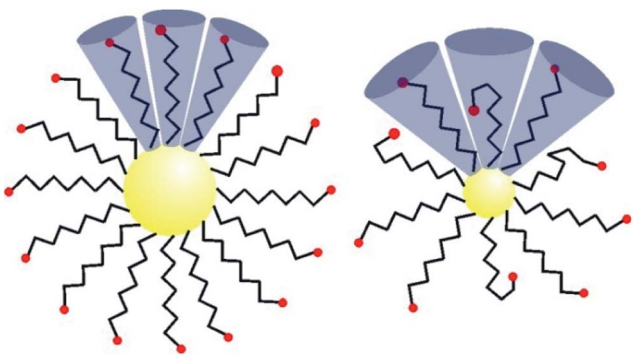

Fig. 1 Schematic drawing of the morphology of ligands on spherical nanoparticles. Due to the spherical geometry of the system, the volume available to the ligands increases with the distance to the surface (blue cones). As the nanoparticle becomes smaller, the ligands can adopt non-all-*trans* conformations in order to explore the additional volume introduced by curvature and, thus, increase their conformational entropy (nanoparticle to the right).

(cylindrical holes with radius much smaller than length) and nanopores[31] (cylindrical holes with radius comparable to length). Polymer chains on concave surfaces can access fewer conformations than those on planar or convex surfaces and thus present interesting nanoconfinement effects.

In a series of papers, Binder and co-workers studied polymer-coated infinite nanochannels using scaling arguments and Monte Carlo (MC) simulations.[28,30] In these studies, chains with an unperturbed radius of gyration much larger than pore radius are predicted to adopt, as expected, conformations consistent with the mushroom and brush regimes for low and high chain surface coverages,[32] respectively. As the cylinder radius decreases, different average conformations result from the strong confinement of the end-grafted polymer chains. Cigar-like conformations (where the chains are elongated in the axial direction) and compressed polymer brushes occur for low and high surface coverages, respectively. The regimes discussed above are predicted for infinitely long nanochannels; in practice, very long-aspect ratio channels (length to radius ratio ~1000) have been prepared by etching ion-tracks in polymer membranes.[33]

Polymers grafted to short pores, such as those prepared by ion or electron-drilling[10,34] show a different behavior to that predicted for infinite channels. In short pores the reservoirs provide additional volume accessible to the chains grafted near the entrances and thus relieve nanoconfinement (Fig. 2a). Fig. 2b and c show the polymer volume fraction and the single-chain volume fraction color maps respectively, obtained with a molecular theory for chains grafted to the center and near the entrance of a polymer-modified short nanopore.[31] The non-zero polymer density in the reservoirs arises from the chains grafted near the entrance (right panel in Fig. 2c) that stretch out of the pore in order to decrease the internal osmotic pressure (*i.e.* increase the solvent volume fraction inside the pore) and to explore the volume of the reservoirs (which translates in a higher conformational entropy and smaller excluded volume interactions). For the surface coverage, chain length and pore radius of the system shown in Fig. 2c, brush-like conformations are expected for infinite cylinders.[28,31] These conformations should be elongated in the direction normal to the walls; however the volume fraction profile for the chain grafted to the center of the short pore in the left panel of Fig. 2c is elongated in the axial direction. This apparent contradiction is explained by the presence of the reservoirs in the short pore, that create additional free volume at pore entrances and favour conformations stretched along the symmetry axis of the pore.[31] This is an example of how details of the geometry at the nanoscale may have very important implications on the molecular organization and therefore they cannot be neglected.

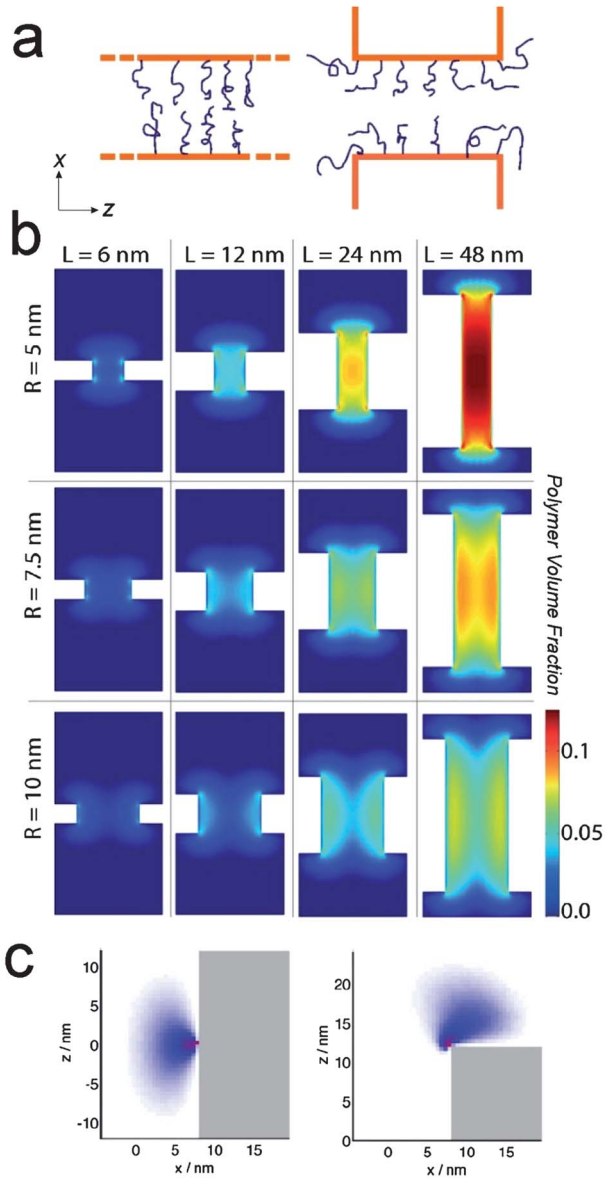

Fig. 2 (a) Schematic diagram for polymer organization in a good solvent regime (no effective segment–segment attractions). Polymer brushes are obtained in long nanochannels for chains with a radius of gyration smaller than channel radius (left). In short nanopores, the presence of the reservoirs allows chains relieving confinement (right). (b) Polymer-segment volume fraction color maps (chain length = 75 monomers per chain; surface coverage = 0.05 chains per nm^2) for different pore dimensions in a good solvent. (c) 2D projections of the average segment density for a single chain within a polymer film. The chains shown are grafted to the center of the pore ($z = 0$, left) or to the edge of the pore ($z = 12$ nm, right). The solid walls of the membrane are shown in grey. The calculations correspond to pore of radius = 7.5 nm; pore length = 24 nm; surface coverage = 0.3 chains per nm^2 and good solvent conditions. Reproduced and adapted with permission from Peleg *et al.*, *ACS Nano*, 2011, **5**, 4737. Copyright 2011 American Chemical Society.

2.2 Self-assembly of end-grafted polyelectrolytes due to microphase separation in the poor solvent regime

An interesting property of polymer and polyelectrolyte end-grafted layers is their ability to microphase separate in poor solvent conditions (where the segment–segment attractions are stronger than the segment–solvent ones) forming aggregates of different shapes.[35–37] Microphase segregation is the result of the competition between attractive short-range interactions and the geometrical constraint introduced by the grafting points that frustrate macroscopic phase separation.[36] In the case of planar surfaces, mean-field theories,[35,37] scaling arguments[36,37] and simulations[37–39] have predicted different morphologies, such as hemispherical micelles, stripes, solvent-filled holes and collapsed

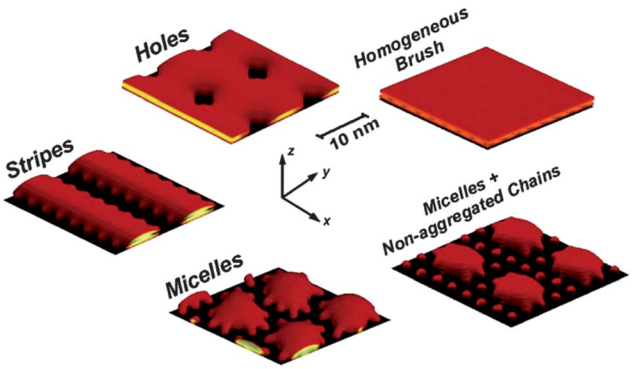

Fig. 3 Morphologies of an end-grafted weak polyelectrolyte planar layer in poor solvent as predicted by a molecular theory. The figures are isodensity surfaces for a polyelectrolyte volume fraction of 0.15 (grafting density = 0.111 chains per nm^2, chain length = 50 segments per chain). The morphology 'micelles + non-aggregated chains' is predicted only for weak polyelectrolyte layers, while the other morphologies are predicted for both weak and strong polyelectrolyte films. Reproduced and adapted with permission from Tagliazucchi *et al.*, *Proc. Natl. Acad. Sci. U. S. A.*, 2010, **107**, 5300.

homogeneous films (see Fig. 3). An interesting novel morphology of micelles coexisting with isolated chains have been predicted in the case of weak polyelectrolytes.[35] Some of these morphologies have been experimentally observed in AFM experiments.[40,41]

Dobrynin and co-workers analysed the phase behavior of nanoparticle-grafted polyelectrolytes in poor solvent using coarse-grain molecular dynamics (MD) simulations.[39] Depending on the strength of the van der Waals (vdW) and electrostatic interactions, different morphologies were predicted (Fig. 4). Collapsed (homogeneous) brushes are found for strong monomer–monomer attractions and weak electrostatic repulsions (which are achieved either by screening of charges in high ionic strength solutions or by counter-ion condensation in very low ionic strength solutions). Bundles of ligands and micelle-like structures (comprising a collapsed-polymer core with condensed counterions and a swollen charged corona) arise for strong monomer–monomer attractions and intermediate ionic strengths. These two morphologies are the result of the balance between electrostatic and vdW interactions. Finally, for weak vdW interactions, a charged polyelectrolyte brush (star-like brush) was obtained. Interestingly, while stripe and hole morphologies are observed for end-grafted polyelectrolyte layers on planar surfaces, equivalent structures were not predicted on nanoparticle surfaces. It is not clear whether this discrepancy arises from the geometry of the system or from differences in the calculation parameters (such as grafting density) or in the molecular model.

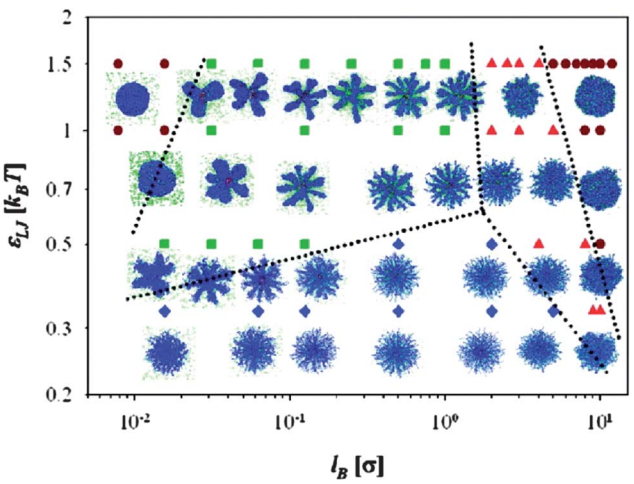

Fig. 4 Morphologies adopted by spherical strong polyelectrolyte brushes: collapsed brushes (circles), bundle brushes (squares), star-like brushes (tilted squares), and micelle-like brushes (triangles) (chain length = 60 monomers per chain, fraction of charged monomers $f = 1/3$). Reproduced and adapted with permission from Sandberg *et al.*, *Langmuir*, 2007, **23**, 12716. Copyright 2007 American Chemical Society.

It is important to emphasize that domain formation in the poor solvent regime is different for weak *vs.* strong polyelectrolytes. This is due to the strong coupling that exists between molecular organization, chemical equilibrium and physical interactions and it leads to qualitatively different phase diagrams and novel morphologies, *e.g.* the micelles and non-aggregated chains, see Fig. 3, where the degree of charge of the chains depends on whether it is in the core or the surface of the micelle.[35]

In poor or mildly poor solvents, long alkyl chains coating small-radii spherical[22] or faceted[42] particles are predicted to form bundles of chains in order to optimize the inter-chain attractive interactions. Stellacci and co-workers have shown the formation of phase-segregated rippled domains in mixtures of short and long thiols on gold nanoparticles.[43,44] MD simulations performed by Glotzer and co-workers suggested that domain formation occurs instead of complete phase separation due to the increase in conformational entropy of long chains adjacent to short ones.[45] The simulations predicted domain formation even for planar surfaces, but stripes were found to form only on spherical particles.

In polymer-modified nanochannels, solvophobic interactions can be used as a tool to control nanoscale morphology and function. For example, the thermoresponsive polymer poly(*N*-isopropylacrylamide), PNIPAM, presents a hydrophilic-to-hydrophobic transition at 32 °C and thus has been used to design temperature-triggered gates in nanochannels[46–48] and nanocages.[49] The conductance of PNIPAM-grafted pores increases above 32 °C; this effect has been ascribed to the collapse of the polymer to the pore walls.[46] A systematic theoretical treatment of the role of solvent quality and pore geometry shows that the collapse-to-the-walls morphology is, however, only one of the possible morphologies predicted for solvophobic polymers in nanopores.[31] The polymer density maps in Fig. 5a show that pore radius, at fixed chain length and surface coverage, controls the morphology of the system and the mechanism of collapse: wide pores (*i.e.* radius larger than the thickness of a collapsed-polymer layer) present aggregates of chains close to the walls (collapse-to-the-walls mechanism). On the other hand, narrow pores display aggregates along the pore axis (collapse-to-the-center mechanism). We believe that the collapse-to-the-walls mechanism is predominant in the experimental literature due to the challenges involved in grafting long chains within narrow nanopores (see Section 4.2). The pore length determines the number of micellar aggregates that form either on the center of the pore or on its walls. For higher grafting densities (not

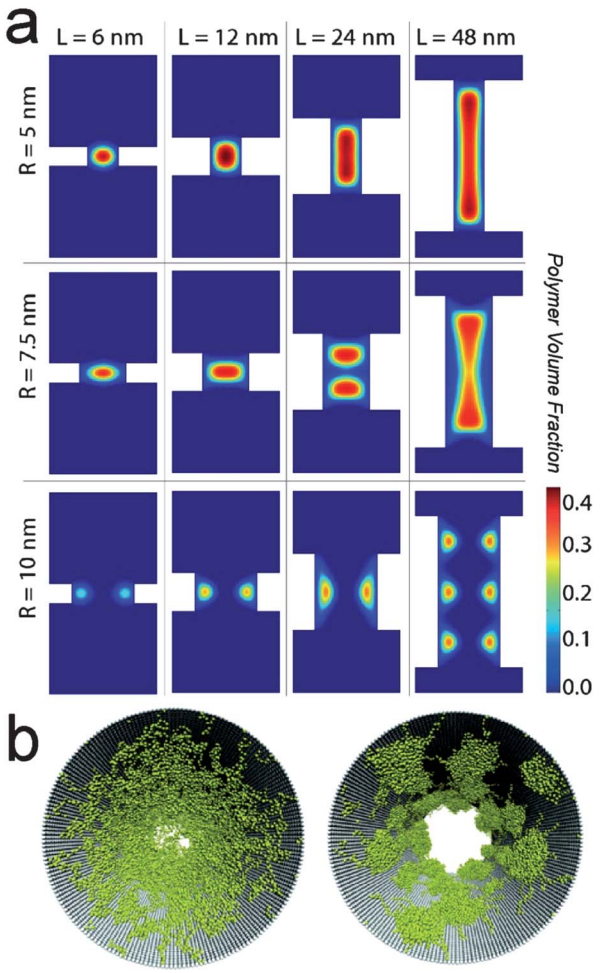

Fig. 5 (a) Polymer volume fraction color maps (chain length = 75 monomers per chain, surface coverage = 0.05 chains per nm^2) for an end-grafted polymer layer within pores of different dimensions in a poor solvent (effective interaction between polymer segments = 1.1k_BT). The color maps show that the polymer chains collapse to the walls of the pore for R = 10 nm and to the center for R = 5–7.5 nm. The pore length controls the number of aggregates. Peleg *et al.*, *ACS Nano*, 2011, **5**, 4737. Copyright 2011 American Chemical Society. (b) Snapshot from a MD simulation of an end-grafted polymer film inside a nanopore for good (left) and poor (right) solvent conditions. In poor solvent regime, the polymer forms micelles on pore inner walls (see Fig. 3). The pore has a radius of 30σ (where σ is the inter-segment distance) and a length of 120σ, the end-grafted chains bear 100 monomers each and are grafted with a surface density of 0.01σ^{-2}. Reproduced and adapted with permission from Adiga *et al.*, *Nano Lett.*, 2005, **5**, 2509. Copyright 2005 American Chemical Society.

shown), continuous rather than micelle-like coatings are predicted on the pore walls or center (depending on pore radius).[31] These results are obtained by assuming a cylindrical-symmetric system, where inhomogeneities can exists only in the radial and axial directions; we expect that future calculations for a completely three dimensional case will enrich the morphological behavior of the system.[50,51] For example, MD simulations performed by Adiga and Brenner showed the formation of pinned micelles of end-grafted polymers on nanopore walls in a poor solvent (Fig. 5b).[51]

3. Chemical equilibrium in nanoconfinement: effects of curvature on apparent acid–base equilibrium constants

Molecular confinement affects the kinetics and thermodynamics of chemical reactions. Therefore, acid–base equilibrium, for example, is coupled to the overall system molecular organization. This coupling may defy our predictive power if it is largely based on equilibrium and rate constants determined in bulk solutions, as well as our chemical intuition developed for homogeneous systems. Namely, the interplay between molecular organization, interactions and chemical equilibrium leads to a non-trivial coupling as will be detailed in the several following examples.

3.1 Chemical equilibrium on nano-curved surfaces

Wang, Nap and co-workers recently studied the acid–base properties of Au nanoparticles coated by the weak carboxylic acid mercaptoundecanoic acid (MUA)[52] (see scheme in the right panel of Fig. 6a). The authors measured the apparent pK_a (pK_a^{app}, defined as the pH where half the carboxylic acid groups on the nanoparticle are deprotonated) from titration experiments for nanoparticles of different sizes and varying salt concentration and types. The plot shows that nanoparticle size and salt concentration affect the pK_a^{app} and that a molecular theory explicitly including size, shape, molecular conformations and chemical equilibrium can quantitatively account for the observed behavior (solid lines in the left panel of Fig. 6a). Fig. 6b shows another system displaying coupled chemical equilibrium and geometry effects: a nanochannel modified by poly(4-vinyl pyridine) (4PVP) chains end-grafted to the inner channel walls. The pyridine segments of 4PVP are weakly basic and can be either in a neutral (pyridine) or protonated (pyridinium) form (see right panel in Fig. 6b). The left panel in Fig. 6b shows the apparent pK_a^{app} predicted by a molecular theory (this theory quantitatively reproduces the experimental pH-dependent conductivity of the channel,[53] see Section 4.3). It is interesting to note that increasing the radius of curvature increases the pK_a^{app} of both the mercaptocarboxylic acids on the gold nanoparticle and the pyridine brush. On the other hand, increasing ionic strength decreases the pK_a^{app} for the pyridine brush in the nanochannel, but decreases that of the carboxylic acids on the gold nanoparticles.

In order to understand the origin of the shift in pK_a^{app} with curvature and ionic strength in the examples of Fig. 6a and b, we should consider the electrostatic repulsion between equally charged groups in dense ligand or polyelectrolyte layers. In order to decrease this electrostatic repulsion, the system opts to regulate its own charge by displacing the acid–base chemical equilibrium to the neutral species (the process where a system decreases its own charge in order to reduce the electrostatic repulsive interactions is known as charge regulation[54,55]). Namely, the system reduces the electrostatic repulsions through the cost in chemical free energy associated with shifting the equilibrium.

Let us analyse the effect of local electrostatics on the protonation–deprotonation equilibria for generic acid and basic groups, namely

$$HA \rightleftarrows A^- + H^+ \quad (1)$$

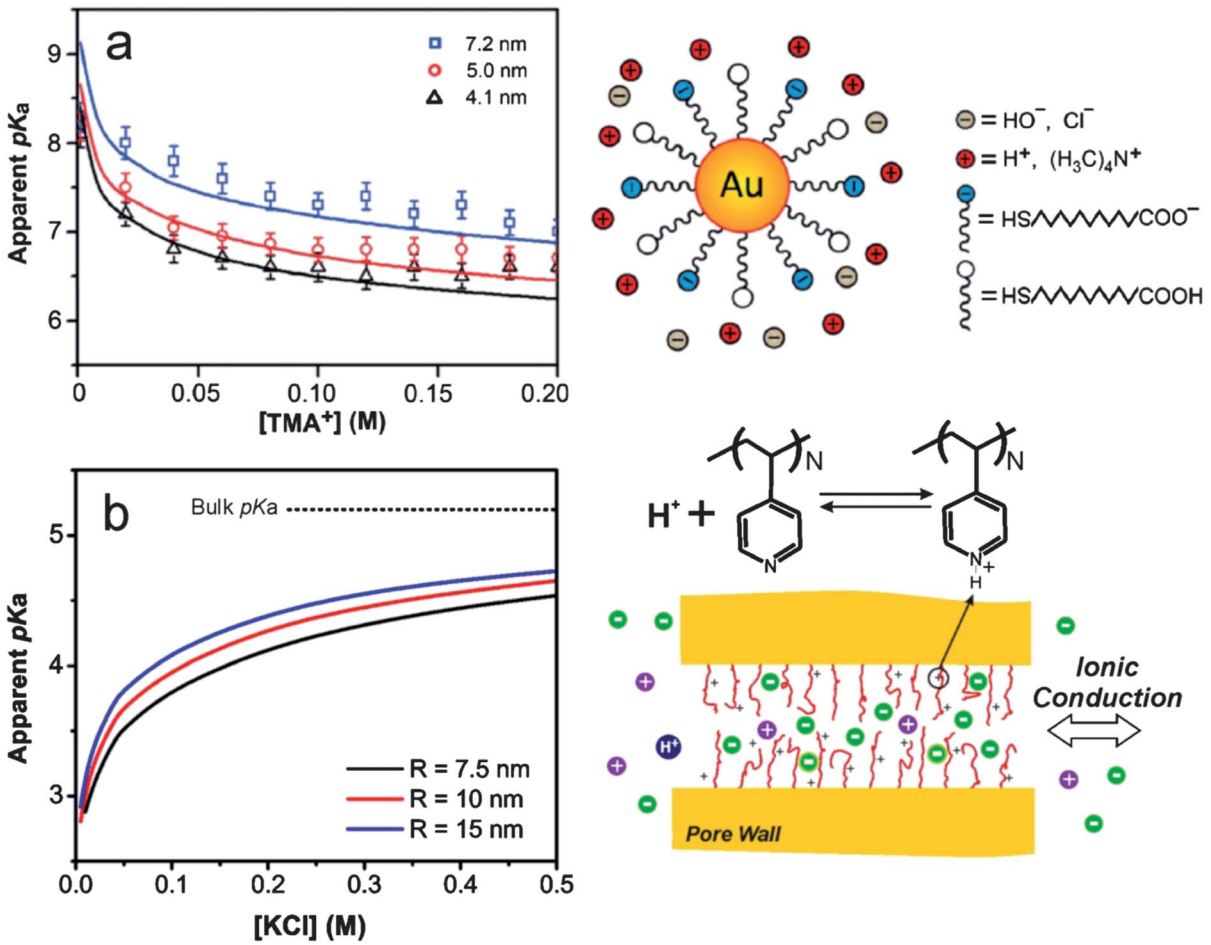

Fig. 6 (a) The apparent pK_a's for the carboxylate headgroup of mercarptocarboxylic acid adsorbed on gold nanoparticles as a function of nanoparticle radius and bulk salt concentration (the right panel shows a schematic drawing of the system). Open markers correspond to experimental data; curves were calculated with a molecular theory. Reproduced and adapted with permission from Wang *et al.*, *J. Am. Chem. Soc.*, 2011, **133**, 2192. Copyright 2011 American Chemical Society. (b) The apparent pK_a's for the pyridine/pyridinium acid–base equilibrium in poly(4-vinyl pyridine) chains end-grafted to the inner surface of a solid-state nanochannel as a function of the channel radius and bulk salt concentration (the right panel shows a schematic drawing of the system). The solid lines are predictions of a molecular theory that successfully reproduces the pH-dependent ionic current through the system (see Section 4.3). The horizontal dashed line indicates the pK_a of an isolated pyridine/pyridinium species in the bulk (the pK_a^{bulk}). The results correspond to surface coverage = 0.2 chains per nm^2 and chain length = 28 segments per chain. Reproduced and adapted with permission from Tagliazucchi *et al.*, *J. Am. Chem. Soc.*, 2010, **132**, 12404. Copyright 2010 American Chemical Society.

$$BH^+ \rightleftarrows B + H^+ \tag{2}$$

The fraction of the charged species in eqn (1) and (2) at a position $\boldsymbol{r}$ (*e.g.* inside the polyelectrolyte brush) can be written as

$$f_{A^-}(\boldsymbol{r}) = \frac{1}{1 + 10^{\left(pK_a^{app}(\boldsymbol{r}) - pH^{bulk}\right)}} \tag{3}$$

$$f_{BH^+}(\boldsymbol{r}) = \frac{10^{\left(pK_a^{app}(\boldsymbol{r}) - pH^{bulk}\right)}}{1 + 10^{\left(pK_a^{app}(\boldsymbol{r}) - pH^{bulk}\right)}} \tag{4}$$

where $pK_a^{app}(\boldsymbol{r})$ is the apparent pK_a at position $\boldsymbol{r}$, given by:[54,56,57]

$$pK_a^{app}(\boldsymbol{r}) = pK_a^{bulk} - \frac{\beta|e|}{2.303}\left(\psi(\boldsymbol{r}) - \psi^{bulk}\right) \tag{5}$$

In eqn (5), $\beta = 1/k_BT$, $|e|$ is the unit of elemental charge and $\psi(\boldsymbol{r})$ is the electrostatic potential at $\boldsymbol{r}$. Note that eqn (3) and (4) resemble the expressions for the dissociation fraction of an acid and a base in solution, with the difference that both the dissociation fraction and the equilibrium constant (pK_a) depend on the position within the system. Eqn (5) shows that, within the model under consideration, the difference between the bulk and the local equilibrium constants is given by the electrostatic potential difference between the two regions. It is important to emphasize at this point that the local electrostatic potential is strongly coupled to the molecular organization and therefore it cannot be independently estimated without the proper treatment of all the molecules involved.[15,54]

The local electrostatic potential within a polyacid layer is more negative than that in the bulk due to the presence of negatively charged deprotonated groups (A^-) and therefore, according to eqn (5), its pK_a^{app} will be higher than the bulk pK_a ($pK_a^{bulk} = 4.8$ for MUA[52] and 5.2 for pyridine/pyridinium[53]). Applying the same argument to a weak polybase results in the opposite behavior, $pK_a^{app} < pK_a^{bulk}$ (see dashed line in the left panel of Fig. 6b). Curvature modulates charge regulation: for convex surfaces, such as the nanoparticles in Fig. 6a, decreasing radius increases the

distance between charged groups and therefore decreases the electrostatic interactions between them (*i.e.* decreases the absolute value of ψ in the polyelectrolyte layer). Therefore, as the radius decreases, the pK_a^{app} shifts towards the pK_a^{bulk}: the pK_a^{bulk} increases for polyacids and decreases for polybases. The opposite behavior holds for concave surfaces as a nanochannel (decreasing radius decreases the distance between charged groups). Finally, salt ions screen repulsions between charges. This effect leads to a higher charge density with lower electrostatic repulsion and therefore increasing the salt concentration shifts the pK_a^{app} towards the pK_a^{bulk}. The shift in the pK_a^{app} due to changes in the ionic strength or curvature are summarized in Table 1 for the different combinations of polyacid–polybase and convex–concave systems.

3.2 Effect of spatial inhomogeneities on chemical equilibrium

The simple qualitative arguments presented in the previous section neglect the inhomogeneous distribution of polyelectrolyte segments within the system. In Fig. 7, we present results from a molecular theory for the polymer distribution in an infinite nanochannel (left panels)[53] and an infinite cylindrical nanotube of the same radius (right panels). The surfaces of both systems are modified by an end-grafted P4VP layer. The nanochannel system is schematized in Fig. 6b and further discussed in Section 4.3. The nanotube example, while not representing a specific experimental system, has similar qualitative features as aggrecans, one of the main components of cartilage.[58,59]

Fig. 7a shows that the volume fraction profiles for both systems are inhomogeneous along the radial coordinate. The polyelectrolyte layer is denser for the nanopore than for the nanotube, which is expected from the fact that the available volume decreases with the distance from the surface for the former and increases for the latter. The positively charged 4PVP segments create a local positive electrostatic potential that follows the shape of the polyelectrolyte density profile. For the cylinder, the electrostatic potential outside the polyelectrolyte layer rapidly decays to its bulk value within a few Debye lengths ($\lambda_D \approx 1$ nm for a 0.1 M 1 : 1 electrolyte solution). For the nanochannel, the electrostatic potential does not decay to its bulk value because the polyelectrolyte chains reach the center of the pore. There is, therefore, an electrostatic potential difference (*i.e.* a 'membrane potential') between the interior of the channel and the bulk solution.

Table 1 Qualitative description of the effect of surface curvature (R) and salt concentration (C_{salt}) on the apparent pK_a of surface-immobilized acid–base species

	Convex surface (sphere or cylinder)	Concave surface (channel, pore or spherical hole)
Polyacid or acid-terminated ligand	$pK_a^{bulk} < pK_a^{app}(R) < pK_a^{app,\ planar}$ $\uparrow R$, $\uparrow pK_a^{app}$ $\uparrow C_{salt}$, $\downarrow pK_a^{app}$	$pK_a^{bulk} < pK_a^{app,\ planar} < pK_a^{app}(R)$ $\uparrow R$, $\downarrow pK_a^{app}$ $\uparrow C_{salt}$, $\downarrow pK_a^{app}$
Polybase or base-terminated ligand	$pK_a^{app,\ planar} < pK_a^{app}(R) < pK_a^{bulk}$ $\uparrow R$, $\downarrow pK_a^{app}$ $\uparrow C_{salt}$, $\uparrow pK_a^{app}$	$pK_a^{app}(R) < pK_a^{app,\ planar} < pK_a^{bulk}$ $\uparrow R$, $\uparrow pK_a^{app}$ $\uparrow C_{salt}$, $\uparrow pK_a^{app}$

Since the electrostatic potential dictates the degree of advancement of the protonation reaction, eqn (2), the shape of the protonation fraction profile of the 4PVP segments follows that of the inverted electrostatic potential. In other words, more positive potentials locally displace the acid–base equilibrium towards the deprotonated neutral species. An important observation is that the protonation fraction is not constant across the polyelectrolyte film. The average value of $f = 0.5$ (solid lines) that results from the choice pH = pK_a^{app} is important because it constitutes the experimental observable variable, but does not necessarily reflect the apparent pK_a^{app} of all segments in the system. An important consequence of spatially inhomogeneous

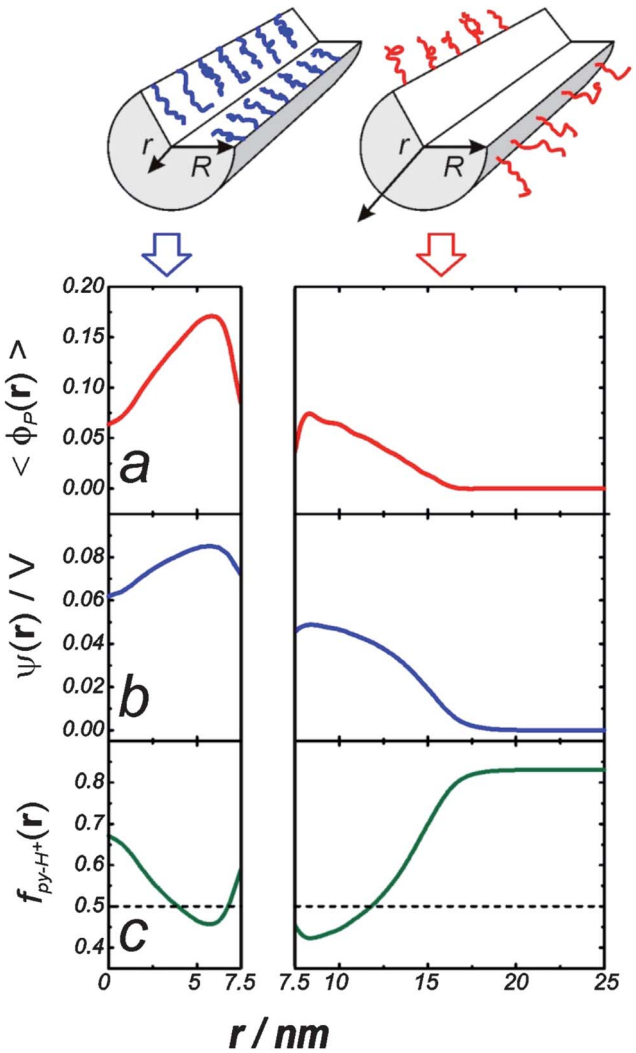

Fig. 7 Radial profiles of polymer volume fraction (a), electrostatic potential (b) and fraction of protonated 4-vinyl-pyridine segments (c) for a 4PVP brush grafted to an infinite channel (left panel) or an infinite cylindrical tube (right panel). The results correspond to pH = pK_a^{app} ($pK_a^{app} = 3.83$ for the nanochannel and $pK_a^{app} = 4.5$ for the nanotube). The dashed line in the lower panels correspond to $f = 0.5$, which is the average fraction of protonated vinyl-pyridine groups. The calculations are for surface coverage = 0.2 chains per nm^2; salt concentration = 0.1 M; $pK_a^{bulk} = 5.2$, radius = 7.5 nm; chain length = 28 segments per chain. Reproduced and adapted with permission from Tagliazucchi *et al.*, *J. Am. Chem. Soc.*, 2010, **132**, 12404. Copyright 2010 American Chemical Society.

chemical environments is that the protonation transition occurs for these systems over a wider range of pH than that expected for the isolated species in the bulk.[53]

We should mention that the effects of charge regulation, nanoconfinement and curvature will affect other chemical/biochemical reactions besides acid–base equilibrium, such as redox equilibrium[57,61,62] (leading to interesting shifts in the electrochemical behavior depending on bulk conditions or aggregate formation[63]) and binding equilibrium.[64] For example, ligand binding on a nanoparticle surface is affected by curvature: the increase of available volume with decreasing radii of curvature favours adsorption on smaller particles. Surface curvature dictates the surface coverages of thiols[65] and DNA oligonucleotides[66] on gold nanospheres and nanorods and also plays an important role in modulating hybridization of nanoparticle-tethered DNA.[67,68]

4. Polymers and polyelectrolytes as molecular gates in solid-states nanopores

The field of polymer- and polyelectrolyte-modified solid-state pores and channels have blossomed over the last years driven by the promise of stimuli responsive nanopores for potential application in sensing,[11] nanofiltration[69,70] and energy conversion.[71,72] Nanochannels modified by synthetic polyelectrolytes,[48,73–77] poly(zwitterions),[78] thermoresponsive polymers,[46,48,79] polypeptides,[80] oligonucleotides[81–83] and lipid layers[84] have been prepared and their conductivity behavior at the single channel level has been characterized. The nanoscale dimensions of solid-state nanopores compete with the length scale of electrostatic interactions and the dimensions of the immobilized macromolecular species; this competition between length scales leads to conductivity behaviors that are not present in microscale fluidic components.[10,85–88]

4.1 Transport of solvent and neutral cargos

Nanofiltration involves transport of solvent and neutral solutes driven by a concentration gradient or an applied pressure. Coating the inner surfaces of porous membranes with end-grafted environment-responsive polymers and polyelectrolytes is a promising avenue to the fabrication of stimuli-gated nanofiltration and delivery devices.

Adiga and Brenner have studied the effect of polymer collapse on solvent flow using MD simulations.[51] In this work, collapse of the polymer layer to the pore walls upon increasing the strength of the segment–segment attractions caused an increase in the pressure-driven flow of solvent through the channel. The authors also theoretically studied a pH-gated flow gate based on the helix–coil transition of grafted polypeptide chains.[89]

Cheng and Cao recently designed a thermo-controlled nanochannel using molecular dynamic simulations.[60] Thermal-responsiveness was introduced by end-tethering chains of ABC triblock copolymer with a solvophilic block between two solvophobic blocks (Fig. 8a) to the pore inner wall. The blocks A and C model a hydrophobic polymer in water (such as polystyrene), while the block B models a charged hydrophilic polymer (like poly(acrylate)). As the temperature increases, the system evolves from a close state to an open state and then back again to a closed state, Fig. 8b–e. At low temperatures, the block C collapses to the center of the channel (Fig. 8b and c), blocking it. The B-block is highly stretched in the collapse-to-the-center morphology and, therefore, there is a big penalty to its conformational entropy. As the temperature increases, the system switches to a collapse-to-the-walls state (Fig. 8d). The aggregates of the block C in the center of the pore are replaced by aggregates formed by the two terminal hydrophobic blocks (A and C) on pore walls. This morphology displays a polymer-free region around the axis of the pore: the pore is in the open state. Finally, for high temperatures, the system seeks to maximize its conformational entropy by forming a swollen layer; this rearrangement of the end-grafted polymers blocks the channel again (Fig. 8e). The authors used non-equilibrium molecular dynamics simulations to show that this open-to-close-to-open process can be used for temperature-tuneable cargo transport.

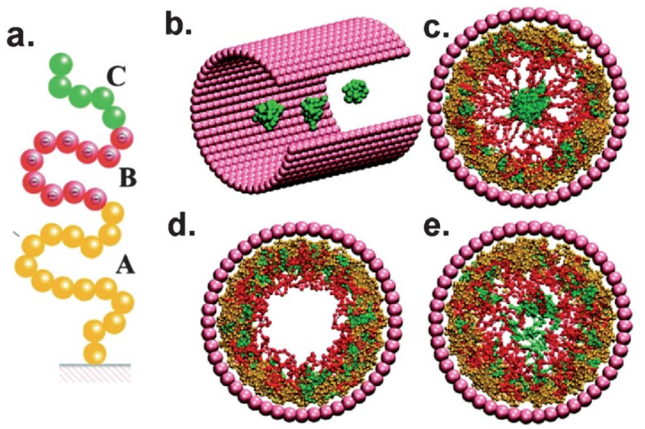

Fig. 8 (a) Schematic diagram of the triblock copolymer studied in ref. 60. Blocks A and C are solvophobic and Block B is solvophilic and negatively charged. The chains are end-grafted to the inner walls of the pore *via* the block C. The parameter ε determined the strength of the interactions between solvophobic segments. (b) Structure formed by block C for $k_BT/\varepsilon = 0.75$ (poor solvent for blocks A and C). Snapshots of the microchannel at different temperatures: $k_BT/\varepsilon = 0.75$ (panel c); $k_BT/\varepsilon = 0.875$ (panel d) and $k_BT/\varepsilon = 1.25$ (panel e). Reproduced and adapted with permission from Cheng *et al.*, *ACS Nano*, 2011, **5**, 1102. Copyright 2011 American Chemical Society.

4.2 Transport and adsorption of polymers inside nanopores

A particularly interesting scenario is that where the macromolecular species flowing through the pore can adsorb to the inner walls. For example, polyelectrolytes are intentionally introduced to modify the inner walls of the pore in the grafting-to and layer-by-layer adsorption methods.[6] Undesired adsorption (fouling) can also occur and ultimately obstruct the pore (clogging).[91]

Koutsioubas *et al.* performed MC simulations to study the formation of polymer end-grafted layers within nanopores *via* the grafting-to method.[90] In the study, chains were initially located in two cubic reservoirs connected by a cylindrical pore (Fig. 9a). In the case where chains can irreversibly adsorb to the surface and cannot undergo lateral diffusion (Fig. 9b), the simulations predict either (i) an homogeneous coating of the pore inner walls for large pore diameters (compared to the unperturbed radius of gyration of the polymer chains) or (ii) a barrier

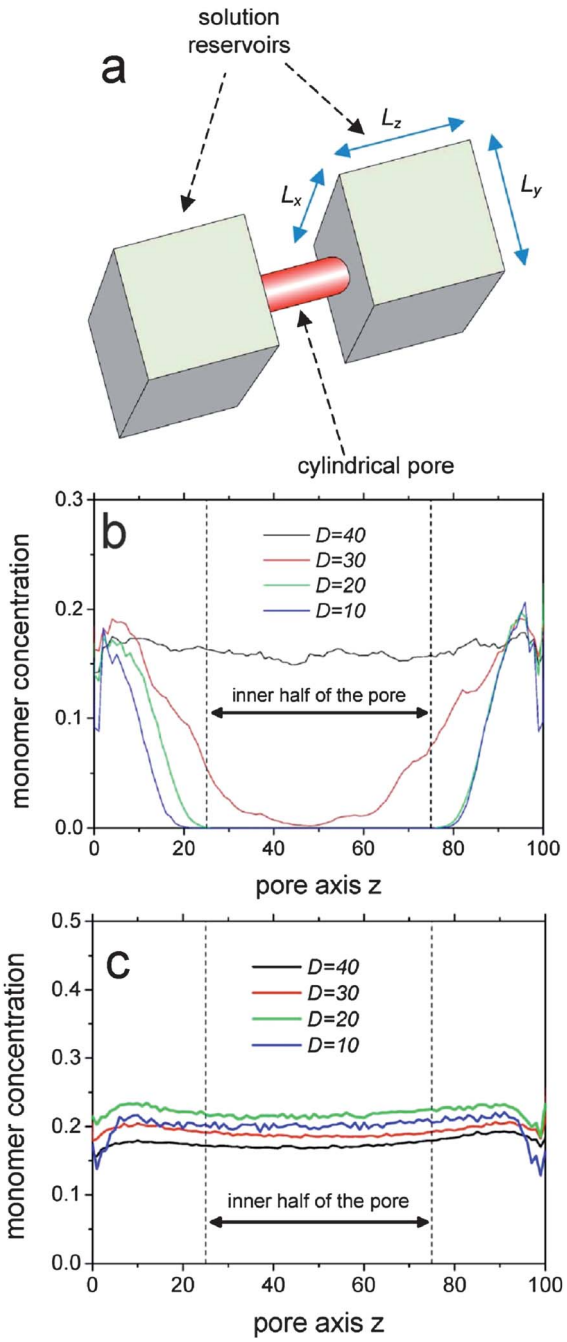

Fig. 9 (a) Schematic drawing of the system studied in ref. 90: a cylindrical nanopore connecting two cubic reservoirs. Freely diffusing chains are located in the cubic reservoirs at the beginning of the simulation. Polymer chains are allowed to bind to the pore inner and outer walls *via* a terminal monomer. (b) Monomer concentration along the pore axis for chains that cannot undergo surface diffusion after binding. Profiles for different pore diameters (D) are shown. For $D < 40$, a barrier is formed on pore entrances that prevent further diffusion of the polymers into the pore. (c) Same as (b), but for chains that can laterally diffuse after binding. Homogeneous polymer coverages inside the pore are obtained for all D. The calculations correspond to a pore length, $L = 100$; chain length, $N = 10$. Reproduced and adapted with permission from Koutsioubas *et al.*, *J. Chem. Phys.*, 2009, **131**, 044901. Copyright 2009 American Institute of Physics.

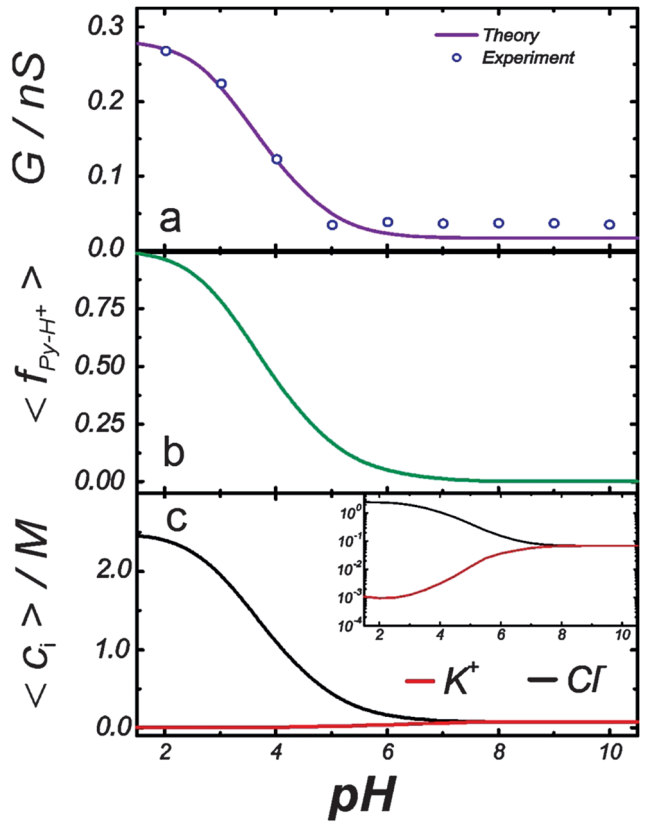

Fig. 10 pH dependence of (a) the conductivity of a nanochannel modified by a poly(4-vinyl pyridine) polyelectrolyte brush (see scheme in the left panel of Fig. 6b). The symbols are the experimental results from Yameen *et al.*[73] and the lines are the predictions from the theory, (b) the average fraction of protonated 4-vinyl-pyridine segments inside the channel and (c) average concentration of salt ions inside the channel (the bulk salt concentration is 0.1 M). The same calculation parameters than Fig. 7 were used in the calculation. Reproduced and adapted with permission from Tagliazucchi *et al.*, *J. Am. Chem. Soc.*, 2011, **133**, 17753. Copyright 2011 American Chemical Society.

at the entrance of the pore for small pore diameters that prevents homogeneous coating of the pore. In the case where the chains can laterally diffuse on the surface after being adsorbed, homogeneous coatings are observed for all pore diameters (Fig. 9c).

Layer-by-layer (LbL) adsorption of oppositely charged polyions into nanoporous substrates is attracting much attention as a source of soft-material tubular architectures.[6] Carrillo and Dobrynin recently reported MD simulations of the LbL assembly of polyelectrolyte–polyelectrolyte, polyelectrolyte–nanoparticle and nanoparticle–nanoparticle layers into cylindrical nanopores.[92,93] The authors found that the film inside the pore rapidly reaches a saturation thickness. In the nanoparticle–nanoparticle and nanoparticle–polyelectrolyte systems, the nanoparticles preferentially deposit at the pore entrance and clog the pore, while in the polyelectrolyte–polyelectrolyte system a plug is formed inside the pore and then it grows towards the entrance. The different behavior of the polyelectrolyte–polyelectrolyte system was ascribed to the flexibility of polyelectrolyte chains. Clogging/saturation effects such as those found in MD simulations has been experimentally observed and avoiding them

remains a major challenge in LbL deposition into nanoporous substrates.[6]

4.3 Transport of ions

Transport of ions and charged macromolecules through nanochannels and nanopores can be driven by an applied electric potential between two non-polarizable electrodes located at the reservoirs.[94] The non-equilibrium problem of ionic conduction through polyelectrolyte-modified nanopores requires modelling the movement of hundreds of ions, solvent molecules and polyelectrolytes in a timescale long enough to guarantee steady-state; this is clearly a formidable task for MD simulations. We have recently tackled the problem by formulating a molecular theory that incorporates a description of ion transport, the degrees of freedom of the immobilized soft materials and the presence of coupled physical interactions and chemical equilibrium.[53,95] This theory allows to address problems beyond the scope of the Nernst–Planck–Poisson (NPP) theory (a continuum approximation commonly used to model bare and surfaced-charged nanopores[96–99]) because it self-consistently treats the presence of grafted polyelectrolytes in the system, includes excluded volume interactions and chemical equilibria and couples electrostatic interactions to the molecular organization and other interactions. All this important couplings are absent in the NPP approach. Briefly, the molecular theory for ion-transport in polyelectrolyte-modified nanopores is based on a generalized diffusion equation for the ions in the system,[95]

$$\boldsymbol{J}_i(\boldsymbol{r}, t) = -D_i\rho_i(\boldsymbol{r}, t)\nabla\beta\mu_i(\boldsymbol{r}, t) \quad (6)$$

where $\boldsymbol{J}_i(\boldsymbol{r}, t)$, $\rho_i(\boldsymbol{r}, t)$, and $\mu_i(\boldsymbol{r}, t)$, are the flux, density and chemical potential of the ion i at position $\boldsymbol{r}$ and time t, respectively and D_i is the diffusion coefficient of the ion i. We couple eqn (6) with a free-energy functional approach in order to determine the organization of the system in the steady-state.[95]

In Fig. 10a we show the experimental pH-dependent ionic conductance through a long nanochannel modified by a layer of end-grafted poly(4-vinyl pyridine) (see the scheme of the system in the right panel of Fig. 6b).[53] Solid lines show that the molecular theory can predict the pH-dependent conductivity through the channel in excellent agreement with the experimental results from Yameen *et al.*[53,73] The pH-dependent conductivity of the system arises from the changes in the concentration of the mobile counter-ions with pH. In low pH solutions, the pyridine segments in P4VP are positively charged (Fig. 10b) and a positive electrostatic environment exists within the pore. Therefore, the concentration of mobile anions (Cl^-) is enhanced inside the pore, while that of the cations is depleted. At pH 2, the concentration of Cl^- within the channel is ~2 M (which should be compared to 0.1 M in the bulk solution); this high concentration of anion charge carriers results in a high-conductivity state (Fig. 10a). As the pH increases, the P4VP segments are deprotonated, the concentrations of Cl^- and K^+ approach their bulk values and the conductance drops. As we explained in Section 3.1, the apparent pK_a of the pyridine units in Fig. 10b ($pK_a^{app} = 3.83$) is lower than the bulk pK_a value of 5.2. The transition between the protonated and deprotonated states is also broader that that expected for an isolated group in the bulk due to the heterogeneous distribution of molecular environments.[53] The concept of inhomogeneous local environments within the pore has been already discussed in Section 3.2.

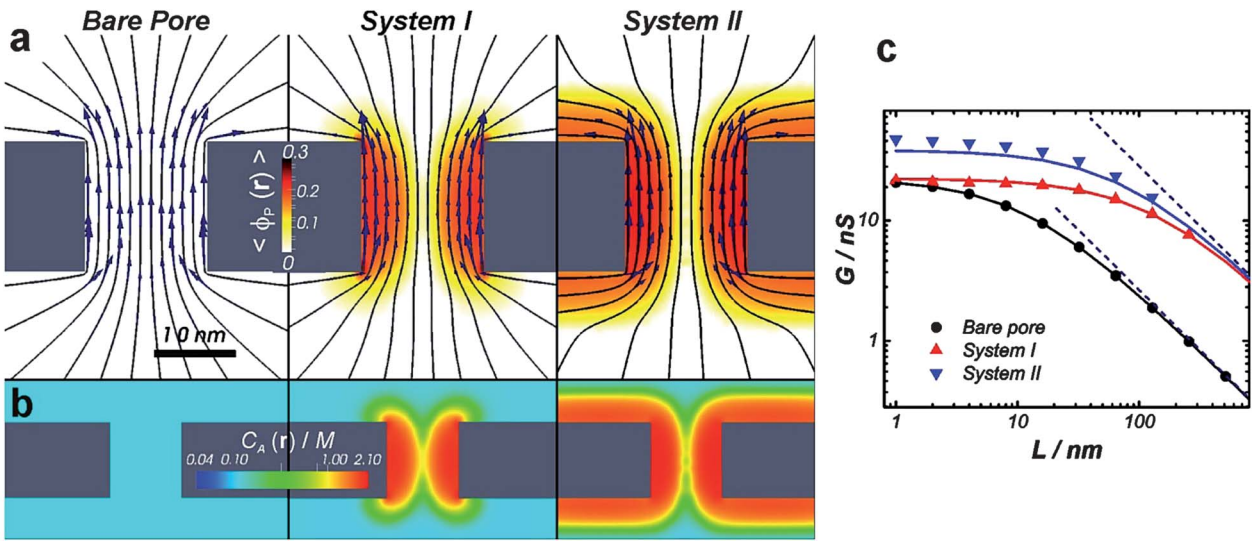

Fig. 11 (a) Polymer volume fraction color maps for a bare short nanopore, a short nanopore that has been modified by positively charged end-grafted polyelectrolytes on the inner pore walls (system I) and a short nanopore that has been modified by positively charged polyelectrolytes end-grafted both to the inner walls and to the outer walls facing the reservoirs (system II). The blue arrows indicate the direction and magnitude of the ionic current flux vectors and the black lines are the flow lines for this vector field. (b) Molar anion concentration color maps for the systems in (a) (note that a logarithmic scale has been used). (c) Ionic conductance of the systems shown in (a) as a function of pore length. Symbols show the predictions of the steady-state molecular theory. Solid and dashed lines are the predictions of simpler conductance models presented in ref. 95, respectively. Calculation parameters: chain length, $N = 20$; charge per monomer, $f = 0.5$; pore radius, $R = 7.5$ nm; bulk salt concentration, $C_{salt} = 0.1$ M, potential bias applied to the reservoirs, $\Delta V = 10$ mV; pore length, $L = 16$ nm (panels a and b only). Reproduced and adapted with permission from Tagliazucchi *et al.*, *J. Am. Chem. Soc.*, 2011, **133**, 17753. Copyright 2011 American Chemical Society.

In Fig. 11, we show the predictions of the theory for a short aspect-ratio nanopore modified by a positively charged polyelectrolyte brush.[95] We present the polymer density color maps (Fig. 11a), ionic current lines (Fig. 11a) and anion concentration color maps (Fig. 11b) for three systems: a bare pore, a pore with a polycation end-grafted only on the inner walls (system I) and a pore with a polycation end-grafted to both inner and outer walls (system II). The arrows on the current flux lines are current vectors that show the direction and magnitude of the total ionic current at each point. The current is boosted in the regions of high polyelectrolyte concentration since these zones possess a high concentration of anions, which act as charge carriers.

Fig. 11c compares the total ionic conductance for the three systems in Fig. 11a as a function of pore length.[95] For very large aspect-ratio pores (nanochannels), the resistance of the pore dominates the total resistance and therefore the conductance decays linearly with pore length. In this regime, the conductances of system I and system II are higher than that of the bare pore because the polyelectrolyte brush enhances the anion concentration within the pore. On the other hand, for very short pores, the resistance of the reservoirs (the access resistance) dominates the total resistance and therefore the conductance is pore-length independent. In this regime, the conductances of system I and the bare pore are the same (because the reservoirs are the same for these two systems), but the conductance of system II is predicted to be higher due to the presence of the polyelectrolyte layer on the outer walls. From the experimental point of view, it is important to note that polyelectrolyte grafting can boost the conductivity of a short pore system by formation of a film on the outer walls, even if the interior of the pore remains unmodified.

The results discussed in previous paragraphs correspond to low ionic currents flowing through the pore. On the other hand, higher ionic currents (achieved by increasing the applied potential bias) can lead to the reorganization of the polymer layer (Fig. 12).[95] For zero current (equilibrium conditions), the polymer is symmetrically distributed with respect to the reservoirs; however, this symmetry is broken for a steady-state finite current. For example, at a steady-state current of 4.5 nA, the positively charged polyelectrolyte chains stretch towards the negatively biased lower reservoir. Chain flexibility controls reorganization: the extent of deformation is very large for long chains (monomers per chain, $N = 60$), but not noticeable for short ($N = 10$) polyelectrolytes. Polyelectrolyte deformation in response to a potential bias in a system of non-polarizable electrodes (such as the reversible Ag/AgCl electrodes typically used in experiments) results from the non-equilibrium electric field sustained by the ionic currents flowing through the pore. This field exerts an electrophoretic force to the end-grafted polyelectrolyte species. Interestingly, Harrell *et al.* have proposed the electrophoretic expulsion/insertion of end-grafted DNA from/to the mouth of a conical nanopores in order to explain the observation of current rectification in that system.[100] The reorganization of the grafted polyelectrolyte layer and mobile ions affects the flux of ions through the system. For instance, the coupling between ion-transport and reorganization are predicted to give rise to non-ohmic behaviors which are sensitive to the properties of the immobilized soft materials.[95]

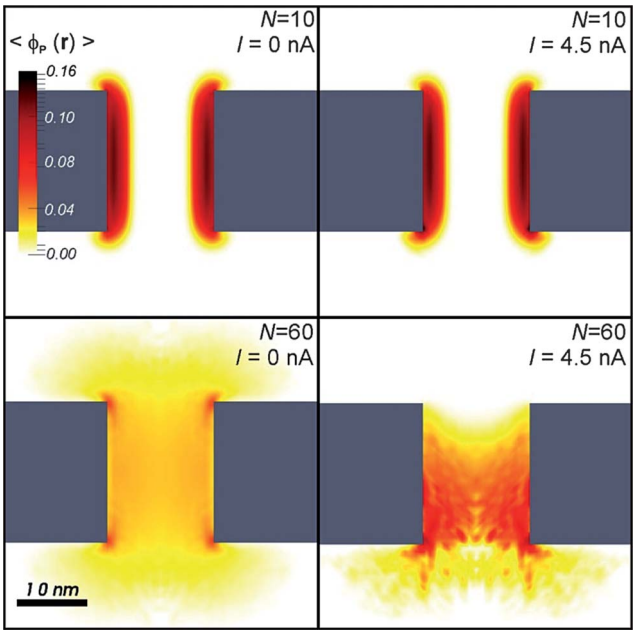

Fig. 12 Polymer volume fraction color maps for a cut along a plane containing the pore axis for a short nanopore modified by positively charged polyelectrolytes end-grafted to the inner walls of the pore. An ionic current I flows through the system as a potential bias is applied between electrodes in the reservoirs (the upped reservoir is positively biased). Results are shown for two different chain lengths (N): long chains ($N = 60$) are deformed upon applying the potential bias and stretch towards the lower (negatively biased) reservoir, while short chains ($N = 10$) are less flexible and do not deform with the applied potential. Reproduced and adapted with permission from Tagliazucchi *et al.*, *J. Am. Chem. Soc.*, 2011, **133**, 17753. Copyright 2011 American Chemical Society.

4.4 A biological polyelectrolyte-modified nanopore: the nuclear pore complex

Recent synthetic efforts have produced the first examples of artificial nanopore gates, but molecular gates more sophisticate than any other ever synthesized already operate in every eukaryotic cell. The nuclear pore complex (NPC, see Fig. 13) is a biological nanopore that controls transport in and out of the cell nucleus.[13,101] The NPC grants the passage to small molecules but blocks cargoes larger than 40 kDa unless they are tagged for transport. Tagged cargoes specifically bind soluble proteins that are known as karyopherins ("kaps"). The interior of the NPC is rich in disorder proteins, which are, in general, depicted either as polyelectrolyte-brush[102,103] or gel-like structures.[104,105] These proteins, the Nups, are rich in the hydrophobic amino acid motif phenylalanine–glycine (FG) and their overall charge is positive. It is believed that the hydrophobic FG domains bind to the kaps through hydrophobic binding spots.[13] However, there is clear evidence also that in order to get into the NPC the proteins need to be hydrophobic and have an overall negative charge.[106]

There is a lack of general consensus on the specific transport mechanism and different investigations have led to different qualitative models.[13] The growing number of experimental studies has set a fertile ground for quantitative theoretical investigations. Miao and Schulten conducted all-atom and

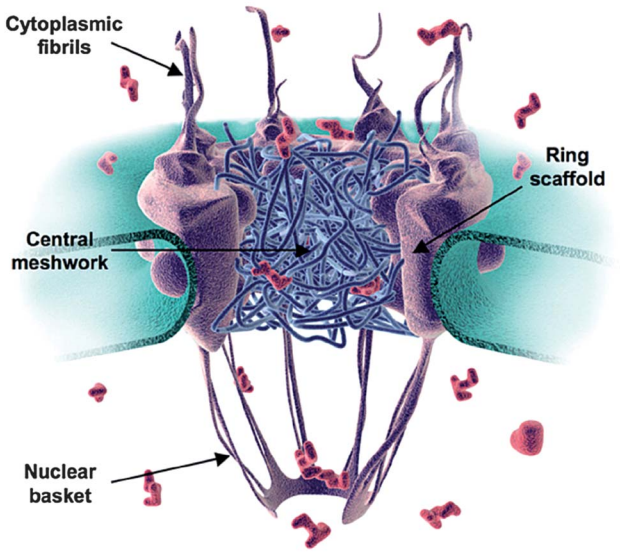

Fig. 13 Schematic drawing of a cross-section of the Nuclear Pore Complex, a large protein complex inserted in the nuclear membrane that controls the transport of biomolecules between the cytoplasm and the interior of the cell nucleus. The characteristic diameter of the pore varies between ~50 to 100 nm, depending on the species. The 'central meshwork' inside the pore is formed by disordered protein filaments rich in phenylalanine–glycine motifs (the FG-Nups). The molecular organization of these proteins and their role during transport are still under debate. Reproduced and adapted with permission from Patel *et al.*, *Cell*, 2007, **129**, 83. Copyright 2007 Elsevier Inc.

coarse grained simulations on planar arrays of Nups and observed brush-like morphologies.[107,108] However, all-atom MD simulations cannot address translocation events, which last a few milliseconds according to the experimental evidence.[109] Therefore, current efforts to model transport are focus on longer-timescale coarse-grain simulations.[110–112] For example, Mincer *et al.* recently proposed that the cargo–karyopherin complex remains bound to a single FG-Nups during its entire trajectory through the pore and it is released in the nuclear side when the cargo–Nups interactions are enzymatically severed.[110] On the other hand, Moussavi-Baygi *et al.* suggested that the kap–FG interaction is highly dynamic and the FG-Nups form a layer on the pore walls.[111,112] The cargo interacts with the FG residues on this layer as it diffuses through the channel. The marked discrepancies between these models clearly result from the choice of the molecular model; these differences are expected since coarse-grain approaches disregard part of the biophysics of the problem (such as the amino acid sequence, geometry of the pore, localization of the Nups within the pore, electrostatics and coupled (bio)chemical reactions). The interesting strong coupling between molecular organization, acid–base equilibrium and molecular organization (*e.g.* domain formation) and their impact on function, *e.g.* ionic conductivity, described in this review points to the need of a detailed molecular description in NPC.

5. Conclusions

Theory and experiment show us that soft materials confined to interfaces behave differently from those in the bulk. In this review, we have discussed how the geometry of the interface affects this molecular environment and makes the properties of surface-confined polymers and polyelectrolytes dependent on curvature.

The morphological regime of polyelectrolyte brushes in a poor solvent is a clear example of qualitatively different behavior arising from the balance between highly non-additive interactions.[35] We have discussed here the morphology diagram of polymer and polyelectrolyte end-grafted to spherical particles and cylindrical pores; however, it is not completely clear whether some of the morphologies predicted for planar layers (*i.e.* stripes, holes, and micelles coexisting with isolated chains) can also exist on nano-curved surfaces. Furthermore, a systematic understanding of the structures that can be obtained on curved objects for polyelectrolytes and weak polyelectrolytes is still incomplete and therefore new morphological regimes may remain undiscovered. In addition to further theoretical work in the area, there is a need of experimental validation for the predicted morphologies, which may be gained from tools such as X-ray/neutron reflectivity techniques[113] and scanning probe microscopies.[40,41,43]

We have discussed the effect of curvature and confinement on chemical-equilibria. These effects are beginning to be well-understood and theoretical predictions are in agreement with experimental measurements. The fundamental lesson is the need for considering the important coupling between molecular organization, chemical equilibrium and physical interactions resulting from their highly non-additive behavior. On the other hand, understanding chemical kinetics in confined environments remains an interesting and important challenge that should be addressed in the future; for example Grzybowski and Stoddart groups recently reported that the switching times for [2]rotaxanes on nanoparticle surfaces depend on nanoparticle size.[4,61]

Dynamical processes in soft materials are of ultimate importance for the description of transport in nanochannels and nanopores modified by supramolecular species. We have reviewed here our approach to the problem of steady-state ion-conduction in polyelectrolyte-modified nanopores.[53,95] However, there are still many open questions and ample room for improvements. For example, the efficiency of mechanical-to-electrical energy transduction in bare nanochannels is determined by the surface charge that controls the ion-selectivity factor.[72,85,97] We have shown that nanochannels modified by 4PVP conduct Cl^- anions with high selectivity[53] and therefore polyelectrolyte-modified nanochannels may outperform the transduction efficiency of bare nanochannels. On the other hand, the presence of the polyelectrolyte layer may block the solution flux through the pore and thus decrease the transduction efficiency. In order to analyse this problem and find an optimal design for energy transduction, a proper treatment of electro-osmotic effects is required. To this end, an approach is needed which includes a description of electrostatics, solvent flow and the conformational properties of the grafted layer. Further work is also necessary to address the effect of non-cylindrical geometries in transport, such as the rectification effects exhibited by polyelectrolyte-coated conical[77,78,83,100,114,115] and biconical pores.[47,48,74,82]

In the final section of this review, we have discussed the exciting prospect of polymers and polyelectrolytes working as gate-keepers for the translocation of large cargoes through

nanopores. We expect that further fundamental studies on transport through polymer-gated pores will shed light on the function of the NPC, serve as guidelines for the design of applications in ultrafiltration, drug-delivery and (bio)analytics and contribute to our basic understanding of biology and the behavior of soft materials in confined environments.

Acknowledgements

We would like to thank our collaborators with whom part of the work presented here has been carried out. This material is based upon work supported as part of the NERC (Non-Equilibrium Research Center), an Energy Frontier Research Center funded by the U.S. Department of Energy, Office of Science, Office of Basic Energy Sciences under Award Number DE-SC0000989.

References

1 M. A. C. Stuart, W. T. S. Huck, J. Genzer, M. Mueller, C. Ober, M. Stamm, G. B. Sukhorukov, I. Szleifer, V. V. Tsukruk, M. Urban, F. Winnik, S. Zauscher, I. Luzinov and S. Minko, *Nat. Mater.*, 2010, **9**, 101–113.
2 M. C. Daniel and D. Astruc, *Chem. Rev.*, 2004, **104**, 293–346.
3 M. Green, *J. Mater. Chem.*, 2010, **20**, 5797–5809.
4 K. P. Browne and B. A. Grzybowski, *Langmuir*, 2011, **27**, 1246–1250.
5 I. Szleifer and R. Yerushalmi-Rozen, *Polymer*, 2005, **46**, 7803–7818.
6 O. Azzaroni and K. H. A. Lau, *Soft Matter*, 2011, **7**, 8709–8724.
7 M. Ballauff, in *Polymer Brushes: Synthesis, Characterization, Applications*, ed. R. C. Advincula, W. J. Brittain, K. C. Caster and J. Rühe, Wiley-VCH, Weinheim, Germany, 2004.
8 D. Vlassopoulos and G. Fytas, in *High Solid Dispersions*, ed. M. Cloitre, 2010, vol. 236, pp. 1–54.
9 G. J. A. A. Soler-Illia and O. Azzaroni, *Chem. Soc. Rev.*, 2011, **40**, 1107–1150.
10 C. Dekker, *Nat. Nanotechnol.*, 2007, **2**, 209–215.
11 S. Howorka and Z. Siwy, *Chem. Soc. Rev.*, 2009, **38**, 2360–2384.
12 W. Sparreboom, A. Van Den Berg and J. C. T. Eijkel, *Nat. Nanotechnol.*, 2009, **4**, 713–720.
13 O. Peleg and R. Y. H. Lim, *Biol. Chem.*, 2010, **391**, 719–730.
14 I. Szleifer and M. A. Carignano, *Adv. Chem. Phys.*, 1996, **94**, 165–260.
15 R. Nap, P. Gong and I. Szleifer, *J. Polym. Sci., Part B: Polym. Phys.*, 2006, **44**, 2638–2662.
16 J. Israelachvili, in *Intramolecular and Surface Forces*, Academic Press, Amsterdam, 2011.
17 E. B. Zhulina, O. V. Borisov and V. A. Priamitsyn, *J. Colloid Interface Sci.*, 1990, **137**, 495–511.
18 R. Nap and I. Szleifer, *Langmuir*, 2005, **21**, 12072–12075.
19 R. L. Jones, N. C. Pearsall and J. D. Batteas, *J. Phys. Chem. C*, 2009, **113**, 4507–4514.
20 M. J. Hostetler, J. J. Stokes and R. W. Murray, *Langmuir*, 1996, **12**, 3604–3612.
21 M. T. Frederick, J. L. Achtyl, K. E. Knowles, E. A. Weiss and F. M. Geiger, *J. Am. Chem. Soc.*, 2011, **133**, 7476–7481.
22 P. K. Ghorai and S. C. Glotzer, *J. Phys. Chem. C*, 2007, **111**, 15857–15862.
23 A. N. Bordenyuk, C. Weeraman, A. Yatawara, H. D. Jayathilake, I. Stiopkin, Y. Liu and A. V. Benderskii, *J. Phys. Chem. C*, 2007, **111**, 8925–8933.
24 M. Daoud and J. P. Cotton, *J. Phys.*, 1982, **43**, 531–538.
25 F. Lo Verso, S. A. Egorov, A. Milchev and K. Binder, *J. Chem. Phys.*, 2010, **133**, 184901.
26 D. Dukes, Y. Li, S. Lewis, B. Benicewicz, L. Schadler and S. K. Kumar, *Macromolecules*, 2010, **43**, 1564–1570.
27 D. Dimitrov, A. Milchev and K. Binder, *Macromol. Symp.*, 2007, **252**, 47–57.
28 D. I. Dimitrov, A. Milchev and K. Binder, *J. Chem. Phys.*, 2006, **125**, 034905.
29 S. A. Egorov, A. Milchev, L. Klushin and K. Binder, *Soft Matter*, 2011, **7**, 5669–5676.
30 R. Wang, P. Virnau and K. Binder, *Macromol. Theory Simul.*, 2010, **19**, 258–268.
31 O. Peleg, M. Tagliazucchi, M. Kroeger, Y. Rabin and I. Szleifer, *ACS Nano*, 2011, **5**, 4737–4747.
32 R. C. Advincula, W. J. Brittain, K. C. Caster and J. Rühe, *Polymer Brushes: Synthesis, Characterization, Applications*, Wiley-VCH, Weinheim, Germany, 2004.
33 N. Chtanko, M. E. Toimil Molares, T. Cornelius, A. Dobrev and R. Neumann, *J. Phys. Chem. B*, 2004, **108**, 9950–9954.
34 A. J. Storm, J. H. Chen, X. S. Ling, H. W. Zandbergen and C. Dekker, *Nat. Mater.*, 2003, **2**, 537–540.
35 M. Tagliazucchi, M. Olvera de la Cruz and I. Szleifer, *Proc. Natl. Acad. Sci. U. S. A.*, 2010, **107**, 5300–5305.
36 D. R. M. Williams, *J. Phys. II*, 1993, **3**, 1313–1318.
37 S. K. Pattanayek, T. T. Pham and G. G. Pereira, *J. Chem. Phys.*, 2005, **122**, 214908.
38 J. M. Y. Carrillo and A. V. Dobrynin, *Langmuir*, 2009, **25**, 13158–13168.
39 D. J. Sandberg, J. M. Y. Carrillo and A. V. Dobrynin, *Langmuir*, 2007, **23**, 12716–12728.
40 V. Koutsos, E. W. van der Vegte and G. Hadziioannou, *Macromolecules*, 1999, **32**, 1233–1236.
41 X. Gao, W. Feng, S. P. Zhu, H. Sheardown and J. L. Brash, *Langmuir*, 2008, **24**, 8303–8308.
42 P. Guo, R. Sknepnek and M. O. de la Cruz, *J. Phys. Chem. C*, 2011, **115**, 6484–6490.
43 A. M. Jackson, Y. Hu, P. J. Silva and F. Stellacci, *J. Am. Chem. Soc.*, 2006, **128**, 11135–11149.
44 A. M. Jackson, J. W. Myerson and F. Stellacci, *Nat. Mater.*, 2004, **3**, 330–336.
45 C. Singh, P. K. Ghorai, M. A. Horsch, A. M. Jackson, R. G. Larson, F. Stellacci and S. C. Glotzer, *Phys. Rev. Lett.*, 2007, **99**, 226106.
46 B. Yameen, M. Ali, R. Neumann, W. Ensinger, W. Knoll and O. Azzaroni, *Small*, 2009, **5**, 1287–1291.
47 W. Guo, H. W. Xia, L. X. Cao, F. Xia, S. T. Wang, G. Z. Zhang, Y. L. Song, Y. G. Wang, L. Jiang and D. B. Zhu, *Adv. Funct. Mater.*, 2010, **20**, 3561–3567.
48 X. Hou, F. Yang, L. Li, Y. L. Song, L. Jiang and D. B. Zhu, *J. Am. Chem. Soc.*, 2010, **132**, 11736–11742.
49 M. S. Yavuz, Y. Cheng, J. Chen, C. M. Cobley, Q. Zhang, M. Rycenga, J. Xie, C. Kim, K. H. Song, A. G. Schwartz, L. V. Wang and Y. Xia, *Nat. Mater.*, 2009, **8**, 935–939.
50 Y. Y. Wu, G. S. Cheng, K. Katsov, S. W. Sides, J. F. Wang, J. Tang, G. H. Fredrickson, M. Moskovits and G. D. Stucky, *Nat. Mater.*, 2004, **3**, 816–822.
51 S. P. Adiga and D. W. Brenner, *Nano Lett.*, 2005, **5**, 2509–2514.
52 D. W. Wang, R. J. Nap, I. Lagzi, B. Kowalczyk, S. B. Han, B. A. Grzybowski and I. Szleifer, *J. Am. Chem. Soc.*, 2011, **133**, 2192–2197.
53 M. Tagliazucchi, O. Azzaroni and I. Szleifer, *J. Am. Chem. Soc.*, 2010, **132**, 12404–12411.
54 B. W. Ninham and A. Parsegian, *J. Theor. Biol.*, 1971, **31**, 405.
55 R. Israels, F. A. M. Leermakers and G. J. Fleer, *Macromolecules*, 1994, **27**, 3087–3093.
56 P. Gong, J. Genzer and I. Szleifer, *Phys. Rev. Lett.*, 2007, **98**, 018302.
57 M. Tagliazucchi, E. J. Calvo and I. Szleifer, *Langmuir*, 2008, **24**, 2869–2877.
58 R. J. Nap and I. Szleifer, *Biophys. J.*, 2008, **95**, 4570–4583.
59 D. Dean, L. Han, A. J. Grodzinsky and C. Ortiz, *J. Biomech.*, 2006, **39**, 2555–2565.
60 L. S. Cheng and D. P. Cao, *ACS Nano*, 2011, **5**, 1102–1108.
61 A. Coskun, P. J. Wesson, R. Klajn, A. Trabolsi, L. Fang, M. A. Olson, S. K. Dey, B. A. Grzybowski and J. F. Stoddart, *J. Am. Chem. Soc.*, 2010, **132**, 4310–4320.
62 M. Tagliazucchi, E. J. Calvo and I. Szleifer, *J. Phys. Chem. C*, 2008, **112**, 458–471.
63 M. Tagliazucchi, E. J. Calvo and I. Szleifer, *AIChE J.*, 2010, **56**, 1952–1959.
64 G. S. Longo, D. H. Thompson and I. Szleifer, *Langmuir*, 2008, **24**, 10324–10333.
65 M. Tambasco, S. K. Kumar and I. Szleifer, *Langmuir*, 2008, **24**, 8448–8451.
66 H. D. Hill, J. E. Millstone, M. J. Banholzer and C. A. Mirkin, *ACS Nano*, 2009, **3**, 418–424.
67 H. D. Hill, S. J. Hurst and C. A. Mirkin, *Nano Lett.*, 2009, **9**, 317–321.

68 K. B. Cederquist and C. D. Keating, *ACS Nano*, 2009, **3**, 256–260.
69 H. Iwata, I. Hirata and Y. Ikada, *Macromolecules*, 1998, **31**, 3671–3678.
70 Y. Ito, Y. S. Park and Y. Imanishi, *Langmuir*, 2000, **16**, 5376–5381.
71 F. H. J. van der Heyden, D. J. Bonthuis, D. Stein, C. Meyer and C. Dekker, *Nano Lett.*, 2007, **7**, 1022–1025.
72 H. Daiguji, P. D. Yang, A. J. Szeri and A. Majumdar, *Nano Lett.*, 2004, **4**, 2315–2321.
73 B. Yameen, M. Ali, R. Neumann, W. Ensinger, W. Knoll and O. Azzaroni, *Nano Lett.*, 2009, **9**, 2788–2793.
74 X. Hou, Y. J. Liu, H. Dong, F. Yang, L. Li and L. Jiang, *Adv. Mater.*, 2010, **22**, 2440.
75 A. Calvo, B. Yameen, F. J. Williams, O. Azzaroni and G. J. A. A. Soler-Illia, *Chem. Commun.*, 2009, 2553–2555.
76 A. Calvo, B. Yameen, F. J. Williams, G. J. A. A. Soler-Illia and O. Azzaroni, *J. Am. Chem. Soc.*, 2009, **131**, 10866–10868.
77 B. Yameen, M. Ali, R. Neumann, W. Ensinger, W. Knoll and O. Azzaroni, *Chem. Commun.*, 2010, **46**, 1908–1910.
78 B. Yameen, M. Ali, R. Neumann, W. Ensinger, W. Knoll and O. Azzaroni, *J. Am. Chem. Soc.*, 2009, **131**, 2070.
79 W. Guo, H. Xia, F. Xia, X. Hou, L. Cao, L. Wang, J. Xue, G. Zhang, Y. Song, D. Zhu, Y. Wang and L. Jiang, *ChemPhysChem*, 2010, **11**, 859–864.
80 Y. Tian, X. Hou, L. P. Wen, W. Guo, Y. L. Song, H. Z. Sun, Y. G. Wang, L. Jiang and D. B. Zhu, *Chem. Commun.*, 2010, **46**, 1682–1684.
81 M. Ali, R. Neumann and W. Ensinger, *ACS Nano*, 2010, **4**, 7267–7274.
82 X. Hou, W. Guo, F. Xia, F. Q. Nie, H. Dong, Y. Tian, L. Wen, L. Wang, L. Cao, Y. Yang, J. Xue, Y. Song, Y. Wang, D. Liu and L. Jiang, *J. Am. Chem. Soc.*, 2009, **131**, 7800–7805.
83 F. Xia, W. Guo, Y. Mao, X. Hou, J. Xue, H. Xia, L. Wang, Y. Song, H. Ji, Q. Ouyang, Y. Wang and L. Jiang, *J. Am. Chem. Soc.*, 2008, **130**, 8345–8350.
84 E. C. Yusko, J. M. Johnson, S. Majd, P. Prangkio, R. C. Rollings, J. Li, J. Yang and M. Mayer, *Nat. Nanotechnol.*, 2011, **6**, 253–260.
85 H. Daiguji, *Chem. Soc. Rev.*, 2010, **39**, 901–911.
86 G. Wang, B. Zhang, J. R. Wayment, J. M. Harris and H. S. White, *J. Am. Chem. Soc.*, 2006, **128**, 7679–7686.
87 A. Plecis, R. B. Schoch and P. Renaud, *Nano Lett.*, 2005, **5**, 1147–1155.
88 D. Stein, M. Kruithof and C. Dekker, *Phys. Rev. Lett.*, 2004, **93**, 035901.
89 S. P. Adiga and D. W. Brenner, *Macromolecules*, 2007, **40**, 1342–1348.
90 A. G. Koutsioubas, N. Spiliopoulos, D. L. Anastassopoulos, A. A. Vradis and C. Toprakcioglu, *J. Chem. Phys.*, 2009, **131**, 044901.
91 P. Stroeve and N. Ileri, *Trends Biotechnol.*, 2011, **29**, 259–266.
92 J.-M. Y. Carrillo and A. V. Dobrynin, *ACS Nano*, 2011, **5**, 3010–3019.
93 J.-M. Y. Carrillo and A. V. Dobrynin, *Langmuir*, 2012, **28**, 1531–1538.
94 M. Muthukumar, *Polymer Tranlocation*, Taylor & Francis Inc, Bosa Roca, 2011.
95 M. Tagliazucchi, Y. Rabin and I. Szleifer, *J. Am. Chem. Soc.*, 2011, **133**, 17753–17763.
96 I. Vlassiouk, S. Smimov and Z. Siwy, *ACS Nano*, 2008, **2**, 1589–1602.
97 I. Vlassiouk, S. Smirnov and Z. Siwy, *Nano Lett.*, 2008, **8**, 1978–1985.
98 P. Ramírez, S. Mafé, A. Alcaraz and J. Cervera, *J. Phys. Chem. B*, 2003, **107**, 13178–13187.
99 I. D. Kosińska, I. Goychuk, M. Kostur, G. Schmid and P. Hänggi, *Phys. Rev. E: Stat., Nonlinear, Soft Matter Phys.*, 2008, **77**, 031131.
100 C. C. Harrell, P. Kohli, Z. Siwy and C. R. Martin, *J. Am. Chem. Soc.*, 2004, **126**, 15646–15647.
101 F. Alber, S. Dokudovskaya, L. M. Veenhoff, W. Zhang, J. Kipper, D. Devos, A. Suprapto, O. Karni-Schmidt, R. Williams, B. T. Chait, A. Sali and M. P. Rout, *Nature*, 2007, **450**, 695–701.
102 R. Y. H. Lim, N. P. Huang, J. Koser, J. Deng, K. H. A. Lau, K. Schwarz-Herion, B. Fahrenkrog and U. Aebi, *Proc. Natl. Acad. Sci. U. S. A.*, 2006, **103**, 9512–9517.
103 R. Y. H. Lim, B. Fahrenkrog, J. Koeser, K. Schwarz-Herion, J. Deng and U. Aebi, *Science*, 2007, **318**, 640–643.
104 S. Frey, R. P. Richter and D. Goerlich, *Science*, 2006, **314**, 815–817.
105 S. Frey and D. Goerlich, *Cell*, 2007, **130**, 512–523.
106 L. J. Colwell, M. P. Brenner and K. Ribbeck, *PLoS Comput. Biol.*, 2010, **6**, e1000747.
107 L. L. Miao and K. Schulten, *Structure*, 2009, **17**, 449–459.
108 L. Miao and K. Schulten, *Biophys. J.*, 2010, **98**, 1658–1667.
109 S. W. Kowalczyk, L. Kapinos, T. R. Blosser, T. Magalhaes, P. van Nies, R. Y. H. Lim and C. Dekker, *Nat. Nanotechnol.*, 2011, **6**, 433–438.
110 J. S. Mincer and S. M. Simon, *Proc. Natl. Acad. Sci. U. S. A.*, 2011, **108**, E351–E358.
111 R. Moussavi-Baygi, Y. Jamali, R. Karimi and M. R. K. Mofrad, *PLoS Comput. Biol.*, 2011, **7**, e1002049.
112 R. Moussavi-Baygi, Y. Jamali, R. Karimi and M. R. K. Mofrad, *Biophys. J.*, 2011, **100**, 1410–1419.
113 S. M. Kilbey and J. F. Ankner, *Curr. Opin. Colloid Interface Sci.*, 2012, **17**, 83–89.
114 M. Ali, B. Yameen, J. Cervera, P. Ramirez, R. Neumann, W. Ensinger, W. Knoll and O. Azzaroni, *J. Am. Chem. Soc.*, 2010, **132**, 8338–8348.
115 M. Ali, B. Yameen, R. Neumann, W. Ensinger, W. Knoll and O. Azzaroni, *J. Am. Chem. Soc.*, 2008, **130**, 16351–16357.

Addition and correction

Note from RSC Publishing

This article was originally published with incorrect page numbers. This is the corrected, final version.

The Royal Society of Chemistry apologises for these errors and any consequent inconvenience to authors and readers.